AIAA SciTech Forum
7-11 January 2019, San Diego, California
AIAA Scitech 2019 Forum

10.2514/6.2019-2070

Thermodynamic and Transport Properties of Hydroxylammonium Nitrate-Based Electric Solid Propellant Vapor

Matthew S. Glascock,[*]
Missouri University of Science and Technology, Rolla, Missouri, 65409, USA

Patrick D. Drew,[†] and Joshua L. Rovey[‡]
University of Illinois Urbana-Champaign, Urbana, Illinois, 61801, USA

Electric solid propellants are advanced solid chemical rocket propellants controlled by electric current. Electric solid propellants may also be used in an electric propulsion system, specifically, an ablative pulsed plasma thruster. Previous experiments with the electric solid propellant HIPEP suggest its ablation processes are similar to traditional propellant polytetrafluoroethylene (C_2F_4). Better understanding of the ablation and resulting propulsion performance of HIPEP requires a model of its vapor composition and transport properties. This paper reports on the development of such a model. The model was validated by comparing results for C_2F_4 with literature, which showed agreement with multiple models described. Transport property results matched within an order of magnitude for temperatures less than 15,000 K and equilibrium composition densities matched to within an order of magnitude. The electric solid propellant vapor composition was predicted in the temperature range of 500-40,000 Kelvin at 1 bar pressure. Low temperatures (<2,000 K) are dominated by H_2O, CO_2 and N_2, and results at 700 K match within 10% of previous combustion model predictions. At high temperatures (>25,000 K) the vapor is strongly ionized and dominated by C^{2+}, O^{2+}, N^{2+}, and H^+ ions. The viscosity of the electric solid propellant vapor is on the order of 10^{-4} kg/m/s and thermal conductivity is on the order of 10 W/m/K.

I. Nomenclature

N	=	number of species in a mixture
G	=	Gibbs free energy, J/kg
μ_j	=	chemical potential of j^{th} species, J/kg-mol
n_j	=	number of moles of j^{th} species
T	=	equilibrium temperature, K
R	=	universal gas constant, J/kg-mol-K
H_j^o	=	standard enthalpy of j^{th} species, J/kg-mol
S_j^o	=	standard entropy of j^{th} species, J/kg-mol-K
n	=	total moles of gas mixture
p	=	pressure of gas mixture, bar
p^o	=	reference pressure for standard thermodynamic table, bar
a_i	=	least-squares regression coefficients for thermodynamic properties, i = 1,2,…,7
b_i	=	least-squares regression integration constants for thermodynamic properties, i = 1,2
Q	=	partition function of a particle

[*] Graduate Research Assistant, Aerospace Plasma Laboratory, Mechanical and Aerospace Engineering, 160 Toomey Hall, 400 W. 13th Street, Student Member AIAA, msgdm3@mst.edu.
[†] Undergraduate Research Assistant, Electric Propulsion Lab, Aerospace Engineering, 6S Talbot Lab, 104 S. Wright Street, Student Member AIAA.
[‡] Associate Professor of Aerospace Engineering, Aerospace Engineering, 317 Talbot Lab, 104 S. Wright Street, AIAA Associate Fellow, rovey@illinois.edu.

M = molar mass of a particle, kg/kmol
k = Boltzmann's constant, J/K
N_A = Avagadro's constant, particles/mol
h = Planck's constant, J-s
Q_{tr} = translational partition function of a particle
Q_{el} = electronic excitation partition function of a particle
m = mass of a particle, kg
g_i = degeneracy of i^{th} ionization state
Θ_i = ionization energy of i^{th} ionization state, eV
η = mixture viscosity, kg/m/s
χ_i = mole fraction of i^{th} gaseous species
η_i = viscosity of i^{th} gaseous species, kg/m/s
ϕ_{ij} = viscosity interaction coefficient of i^{th} gaseous species with j^{th} gaseous species
$\bar{\Omega}^{(2,2)}(T)$ = collision integral at specified temperature, T
λ_{fr} = frozen contribution to mixture thermal conductivity, W/m/K
λ_i = thermal conductivity of i^{th} gaseous species, W/m/K
ψ_{ij} = thermal conductivity interaction coefficient of i^{th} gaseous species with j^{th} gaseous species
c_v = gas specific heat capacity at constant volume, J/K
λ_{tr} = thermal conductivity of a gas mixture due to translational energy, W/m/K
λ_{int} = thermal conductivity of a gas mixture due to internally stored energy, W/m/K
λ_{re} = thermal conductivity of a gas mixture due to chemical reactions, W/m/K
λ = total thermal conductivity of a gas mixture, W/m/K

II. Introduction

Recent innovation in the solid rocket propellant field has led to the development of electric solid propellants (ESPs) that are safe, throttle-able, green propellants. ESPs ignite and decompose when electric power is applied at sufficient current and voltage[1-3]. This decomposition is a highly exothermic process that generates hot gas at a burn rate that can be throttled by the applied current. Removal of the voltage and current extinguishes the reaction, at which point the reaction may be restarted by reapplication of electric power. Because this reaction is induced only by electric current, ESPs are not susceptible to accidental ignition by spark, impact or open flame. These characteristics are extremely beneficial compared to traditional solid rocket propellants, which are not throttle-able, toggle-able or insensitive to external ignition. The advent of ESPs expands the potential applications for solid propellant into areas previously infeasible, such as attitude control for small spacecraft or use in a dual-mode device.

Recent development of ESPs has led to the creation of a high performance electric propellant known as HIPEP. In this solid energetic material, the ionic liquid oxidizer hydroxylammonium nitrate (HAN) exhibits pyroelectric behavior unique to energetics. When electric power is applied, the proton transfer reaction between hydroxylammonium and nitrate is promoted, and the level of nitric acid rapidly rises in the material, eventually triggering ignition of the propellant. This behavior may enable HIPEP to be used in a dual-mode propulsion system, wherein a high thrust chemical mode, using direct current to incite high temperature pyroelectric gas generation, is paired with a high efficiency electric mode. One promising electric mode configuration is a pulsed electric propulsion device known as the ablation-fed pulsed plasma thruster (APPT). HIPEP and similar propellants have been tested as APPT propellants in Aerojet's modular test unit (MTU). Results from those tests reported impulse bits within 50% of the traditional APPT propellant, polytetrafluoroethylene (PTFE) [3].

Pulsed plasma thrusters[4] (PPTs) have been in use since the first orbital flight of an electric propulsion device in 1968. PPTs offer repeatable impulse bits with higher exhaust velocities than possible using chemical thrusters, so long as electric power is already available on the spacecraft. The traditional PPT propellant is PTFE, which is a solid that is ablated during the electrical discharge to yield a conductive plasma working fluid. APPTs have the added benefit of inert propellant storage with no pressure vessel requirements. The solid propellant typically fills the space between two electrodes. A capacitor or bank of capacitors is charged to a few kilovolts across the electrodes and an arc discharge is initiated by an ignitor. This arc discharge is fueled by ablation from the surface of the solid propellant, and consequently heats ablated propellant vapor to high temperature. Ablation processes are at the core of APPT operation, and thus many studies on the ablation of PTFE exist in literature[5-11]. Empirical studies have shown that the specific ablation, that is the ablated mass relative to the energy stored on the capacitor bank, is typically 1.5-10 μg/J for PTFE-fed PPTs of various geometries[4]. In a single PPT pulse, it has been estimated that >40% of the mass lost is ablated in the form of slow macroparticles or late-time ablation, which reduces propellant utilization efficiency[5,12].

Our recent work has compared the ESP HIPEP with traditional PTFE in a PPT test article[13-17]. At high temperatures and over long (~ms) time-scales, it is known that HIPEP undergoes a thermal decomposition process, while PTFE evaporates after depolymerization. However, ablation processes present in APPTs occur on much shorter timescales, as the discharge current has a period of less than 10 μs. LCR circuit model analysis has shown that the conductivity of the HIPEP material does not affect the discharge current significantly[13]. The specific ablation of HIPEP is roughly twice that of PTFE, but on the same order of magnitude. This difference in ablation mass between the two propellants can be directly attributed to differences in the material thermal and chemical properties[14]. Plume measurements of these same HIPEP microthrusters indicate electron temperatures (1-2 eV) and densities (10^{11}-10^{14} cm^{-3}) of the weakly ionized plasma comparable to that of PTFE fueled APPTs[15]. Exhaust velocity measurements indicate similar performance of HIPEP relative to PTFE in the microthrusters. Further, it has been shown that the fraction of late-time ablation mass is similar between propellants. Estimates from high-speed imagery from a pulsed HIPEP microthruster suggest that up to 50% of the mass ablated may be attributed to low-speed macroparticles ejected after the main current pulse[16].

Many efforts to model the ablation of PTFE can be found in literature with context to PPT propellant as well as for high voltage circuit breakers. The previous experimental results comparing HIPEP and PTFE suggest that these same ablation and PPT performance models can be used to describe the HIPEP material, so long as the differences in material properties are accounted for. One such PPT ablation and performance model by Keidar and Boyd[18,19] agrees quantitatively with empirical results for a coaxial APPT with solid PTFE propellant. Among the key inputs to this model, and into bulk plasma models describing density and temperature, are the equilibrium chemical composition and transport properties of the propellant vapor that constitutes the plasma. Such models exist for PTFE using various methods[20,21], but none exist for HIPEP, or even its primary constituent, HAN. Future HIPEP characterization and modeling requires a thermochemical model for the HIPEP as a high temperature vapor plasma. Then an ablation model similar to that used for PTFE may be constructed for the ESP HIPEP.

Thermochemical models are typically obtained via one of two methods. First, examination of the equilibrium constants of a set of reactions can account for two-temperature effects and condensed phases readily, but requires knowledge of the specific elementary and reduction reactions for all species. Second, a Gibbs free energy minimization method for the system of individual species is less complex for increased numbers of species as the species may be treated individually without knowledge of the reactions. Both methods have been applied to PTFE (pure C_2F_4 gas) in the range of 1,000-40,000 Kelvin[20-22]. The specific set of reactions for the constituents of the HIPEP material are not currently known, thus we have elected to apply the Gibbs free energy method. In this work, we use the Gibbs free energy minimization method to determine the equilibrium chemical composition of HIPEP vapor at 1 bar pressure over a temperature range of 500-40,000 K. The Chapman-Enskog approximation method is then used to determine transport properties of the propellant vapor at these conditions. Our model is validated by simulating PTFE vapor, and then comparing our results with literature. Thermogravimetric analysis is used to examine the vaporization temperature for each material, yielding appropriate low temperature bounds. Further, predicted HIPEP vapor composition is compared to other work for a low temperature. Observed differences in the composition and transport property predictions for PTFE versus HIPEP are highlighted and discussed.

III. Theoretical Development

First, the theory of the Gibbs free energy minimization method for determining the chemical composition of a gas at equilibrium is reviewed. Second, a brief discussion of the Chapman-Enskog approach to approximate thermodynamic transport properties is described. Finally, details concerning the chemical makeup and component gas species for each propellant material are presented.

A. Equilibrium Chemical Composition

The method of minimizing the Gibbs free energy of a chemical system to determine its equilibrium state is a commonly used approach. In 1994, Gordon and McBride published a NASA report detailing the methods used in the Chemical Equilibrium with Application (CEA) computer program[23,24]. This method was followed in the current work to obtain the chemical composition of the given gaseous mixture at local thermal and chemical equilibrium using a modified form of the NASA CEA program available online[24]. The Gibbs free energy per kilogram of a mixture of N species is defined as

$$G = \sum_{j=1}^{N} \mu_j n_j \tag{1}$$

Here μ_j is the chemical potential per kg-mol and n_j is the number of moles of the j^{th} species, respectively. Using a descent Newton-Rhapson method, Eq. (1) is minimized, subject to mass and charge balance constraints. The chemical potential of species j is given by

$$\mu_j = H_j^o(T) - TS_j^o(T) + RT\ln\left(\frac{n_j}{n}\right) + RT\ln\left(\frac{p}{p^o}\right) \tag{2}$$

In Eq. (2), R is the universal gas constant, T is the equilibrium temperature of the gas mixture in Kelvin, and p/p^o is the ratio of the mixture pressure to the reference pressure. Finally, $H_j^o(T)$ is the standard enthalpy and $S_j^o(T)$ is the standard entropy of species j at temperature T, respectively. Thermochemical properties of many individual species are available in the JANNAF tables for temperatures up to 6,000 K. Data from the fourth edition of the JANNAF tables[25] are included in the CEA program in the form of least squares fits, and were used in the present work. In this edition, the reference pressure is stated as 1 bar for all species and we choose to use 1 bar as the assigned mixture pressure, eliminating the final term in equation (2). These fits are provided in seven coefficients (a_{1-7}) and two integration constants ($b_{1,2}$) of the form

$$\frac{H_j^o}{RT} = -a_1T^{-2} + a_2T^{-1}\ln(T) + a_3 + \frac{a_4}{2}T + \frac{a_5}{3}T^2 + \frac{a_6}{4}T^3 + \frac{a_7}{5}T^4 + \frac{b_1}{T} \tag{3a}$$

$$\frac{S_j^o}{R} = -\frac{a_1}{2}T^{-2} - a_2T^{-1} + a_3\ln(T) + a_4T + \frac{a_5}{2}T^2 + \frac{a_6}{3}T^3 + \frac{a_7}{4}T^4 + b_2 \tag{3b}$$

For most species, fits were provided for two temperature intervals, 200-1,000 K and 1,000-6,000 K. The higher temperature fit was extrapolated for use in the present work. The data fits were used directly for all available species in these temperature intervals. The monatomic species also had fits provided for the 6,000-20,000 K interval, which were used directly in that temperature interval, and linearly extrapolated to 40,000 K. Data from a separate model were included in the program for the doubly-ionized species, which are not included in the JANNAF tables. For ideal ions the thermochemical properties can be related to the partition function Q by[20]

$$\frac{H_j^o}{RT} = T\frac{d(\ln Q)}{dT} + \frac{5}{2} + \frac{H_0^o}{RT} \tag{4a}$$

$$\frac{S_j^o}{R} = T\frac{d(\ln Q)}{dT} + \ln Q + \frac{3}{2}\ln M + \frac{5}{2}\ln T + \frac{5}{2} + \ln\left[k\left(\frac{2\pi k}{N_A h^2}\right)^{\frac{3}{2}}\right] \tag{4b}$$

where the partition function can be written as the sum of the translational and electronic contributions as[26]

$$Q = Q_{tr} + Q_{el} = \left(\frac{2\pi mkT}{h^2}\right)^{\frac{3}{2}} + \left[g_0 + g_1\exp\left(-\frac{\Theta_1}{T}\right) + g_2\exp\left(-\frac{\Theta_2}{T}\right)\right] \tag{5}$$

Here, the electronic state degeneracies ($g_{0,1,2}$) and ionization energies ($\Theta_{1,2}$) were obtained from the NIST atomic spectra database[27]. Equations (4) and (5) were used to generate date in the same form as presented in the JANNAF tables. A reduced form of equation (3) with all coefficients set equal to zero except a_3, b_1, and b_2 is then fit to the thermodynamic data for only these doubly ionized species. The resulting fit is similar in shape to the provided fit for electron gas and singly-ionized species. This fitting process is achieved by use of a multiple non-linear regression algorithm to generate values for the three least-squares coefficients.

B. Transport Properties

Transport coefficients of a vapor mixture are typically calculated based on the Chapman-Enskog approximation of the Boltzmann equation. The rigorous method is detailed in Hirshfelder, Curtiss and Bird[28]. In the present work, a first-order approximation is used for viscosity and the second-order approximation for thermal conductivity, following the work of Gordon et al.[29] that is integrated within the NASA CEA program. This method approximates the viscosity η of a mixture of N gases as

$$\eta = \sum_{i=1}^{N}\frac{\chi_i\eta_i}{\chi_i + \sum_{j=1,j\neq i}^{N}\chi_j\phi_{ij}} \tag{6}$$

Here χ_i are the mole fractions of each species, ϕ_{ij} are the interaction coefficients given by Gordon et al.[29], and the viscosity of each species η_i may be written

$$\eta_i = \frac{5}{16}\frac{(\pi m k T)^{\frac{1}{2}}}{\bar{\Omega}^{(2,2)}(T)} \tag{7}$$

which depends on the species mass m, the temperature, and the value of the collision integral $\bar{\Omega}^{(2,2)}$ for the given temperature. The collision integrals are approximated using the approach detailed by Svehla and McBride[30].

Calculation of the thermal conductivity is split into two calculations of the frozen and reaction thermal conductivity. The mixture frozen thermal conductivity λ_{fr} is determined similarly to viscosity by

$$\lambda_{fr} = \sum_{i=1}^{N} \frac{\chi_i \lambda_i}{\chi_i + \sum_{j=1, j\neq i}^{N} \chi_j \psi_{ij}} \tag{8}$$

Here ψ_{ij} are a separate set of interaction coefficients detailed in Gordon et al.[29] and λ_i are the species thermal conductivities which may be determined by

$$\lambda_i = \frac{25}{32}\frac{c_v(\pi m k T)^{\frac{1}{2}}}{\bar{\Omega}^{(2,2)}(T)} \tag{9}$$

where c_v is the gas specific heat capacity at constant volume. The thermal conductivity of each species is largely dependent on the species temperature and c_v, which differs between monatomic and polyatomic species. Each species' thermal conductivity calculation includes the translational energy contribution (λ_{tr}) as well as the contribution from any internally stored energy (λ_{int}) in the case of polyatomic species. The reaction contribution to the mixture thermal conductivity λ_{re} is dependent on the heat of reaction for each dissociation or ionization reaction within the mixture, and may be added to the frozen contribution like so

$$\lambda = \lambda_{tr} + \lambda_{int} + \lambda_{re} = \lambda_{fr} + \lambda_{re} \tag{10}$$

where λ is the desired total thermal conductivity of the gas mixture. Thermal transport property data for many species are included in the CEA program in the form of least-squares fit coefficients. These four coefficient fits are derived from literature data for a handful of the species considered in the present work and the data included in the program were not modified.

C. Propellant Composition

Accurate prediction of the chemical composition requires careful consideration of the constituent species used to model each of the propellants. Here the selected species and relative weights input to the thermochemical model are described. The PTFE samples in this work are purely polytetrafluoroethylene, a non-conductive polymer. Thermal degradation of this polymer is characterized by the "unzipping" of the chain into the monomer, in this case C_2F_4. Using thermogravimetric analysis (TGA) coupled with Fourier-transform infrared spectroscopy (FTIR), Schild[31] observed almost exclusive production of C_2F_4 during thermal degradation of PTFE. For our thermochemical model, we have selected to define the constituent species of PTFE as 100% C_2F_4 by weight, as shown in Table I.

Table I: Selected model constituent species and mass fractions for each propellant.

Material	Constituent Species Name	Chemical Formula	Relative Weights	Molar Mass, g/mol
PTFE	Tetrafluoroethylene	C_2F_4	1.0000	100.02
HIPEP	Nitric Acid	HNO_3	0.4921	63.01
	Hydroxylamine	NH_2OH	0.2579	33.03
	Acetaldehyde	CH_3CHO	0.2000	44.05
	Ammonium Nitrate	NH_4NO_3	0.0500	80.04

The ESP is a mixture of more complex species and care must be taken when selecting the constituent species used in the model. HIPEP is a HAN-based solution solid manufactured by Digital Solid State Propulsion (DSSP) using "green" ingredients and processes free of harmful fumes. It is mixed in liquid form in standard chemical glassware, with only gloves and safety glasses needed for protection, and cures at room temperature (35°C/95°F), forming a soft solid with the appearance and texture of a soft pencil eraser. HIPEP has a chemical composition of 75% HAN oxidizer (an inorganic ionic liquid), 20% polyvinyl alcohol (PVA) fuel binder, and 5% ammonium nitrate[13,17]. The

thermodynamic and transport properties of the primary constituent, HAN, in vapor form are not well known because the material does not evaporate like PTFE and many other materials. What is known, however, is that solid and aqueous HAN undergoes a thermal decomposition process at temperatures above 400 K. Lee and Litzinger[32] conducted a thermal degradation experiment with aqueous solutions of HAN and found that a reaction producing hydroxylamine (NH_2OH) and nitric acid (HNO_3) initiates the thermal decomposition process. The timescale for this initiation reaction was estimated to be on the order of 10^{-10} seconds. A typical PPT current pulse has a period on the order of 10^{-6} seconds, which means this reaction occurs on a timescale short enough for these species to dominate the plume composition. Because the propellant undergoes this decomposition to transition to the vapor phase in which we are interested, these species were chosen (in relative weights equivalent to 75% HAN) to model the main constituent of the HIPEP material. The fuel binder, PVA (CH_2CHOH), is a synthetic polymer and water-soluble. Like HAN, the thermodynamic and transport properties of PVA vapor are not well known, as the material is typically in solid or aqueous form. At room temperature, acetaldehyde (or "ethanal") is a more stable form of the molecule with a mobile proton and has the idealized formula of CH_3CHO. We have selected to use this material to model the PVA constituent. The final 5% of the ammonium nitrate in the HIPEP material is modeled using the known properties of ammonium nitrate, NH_4NO_3. The chosen constituent species and their relative weights for the HIPEP material model are shown in Table I.

IV. Model Validation

First, the thermal degradation temperature for PTFE and HIPEP are examined using experimental data. Second, the results obtained using the described thermochemical model for polytetrafluoroethylene are compared to the works of other researchers using similar methods. Third, results for the ESP at a single low temperature are compared to other researchers' results at that temperature using similar methods. These comparisons illustrate the accuracy of the model presented here relative to the models presented in the literature.

A. Thermal Degradation Temperature

The upper bound of the temperature range in the thermochemical model in the present work was somewhat arbitrarily chosen to cover the range of electron temperatures typically measured in PPT plumes[4], i.e. 1-3 eV. Selection of the lower bound requires more careful consideration. If the lower bound is chosen below the vaporization temperature of the material, the Gibbs minimization method may not converge. In cases where it will converge, the theoretical results obtained would be meaningless in the consideration of a real vapor. The present work thus included a brief study of the thermal degradation temperature (i.e. the temperature that incites vapor production) for the materials considered using thermogravimetric analysis.

Thermogravimetric analysis (TGA) is a material science technique wherein the weight of a small material sample is measured during heating of the sample. In our tests, the heating rate (K/min) is held at a predetermined constant rate for the duration of the test, and sample weight is measured over time. Results are typically presented in terms of measured weight percent with respect to temperature and/or the derivative of sample weight versus temperature. In the present work, the Q50-TGA model from TA Instruments was employed, which has a maximum mass balance capacity of 1000 mg and sensitivity of 0.1 μg. PTFE and HIPEP were tested in the apparatus with sample sizes varying between 10 and 20 mg. These samples were cut into many thin pieces 2 or 3 mg in mass to maximize the surface area-to-mass ratio, allowing even heating and evaporation. After a system tare with a platinum platter and 90 μL alumina crucible was complete, a sample was loaded into the crucible. Nitrogen gas was delivered by a separate gas inlet tube such that the sample was contained in an inert environment at atmospheric pressure for the duration of the test. After each experiment and data collection, the sample cup was removed from the system and remaining sample was collected. All PTFE tests resulted in complete decomposition and no remaining sample. HIPEP tests produced a black solid of 10%-20% the original sample weight. The exact composition of the residual solid is currently unknown, but is suspected to be largely carbon.

Figure 1a presents the TGA curves for two samples of PTFE tested in the present work. Also plotted are results from Hondred et al.[33] for two samples of PTFE analyzed using TGA. There is a clear separation between onset temperature (where sample weight begins to decrease) and full thermal degradation (sample weight is zero) for PTFE TGA curves, indicating a rapid, single-step degradation. Further, the TGA curve is shifted to higher temperatures for increased heating rate. Comparison of our results with that in literature shows agreement within 3% for both heating rates.

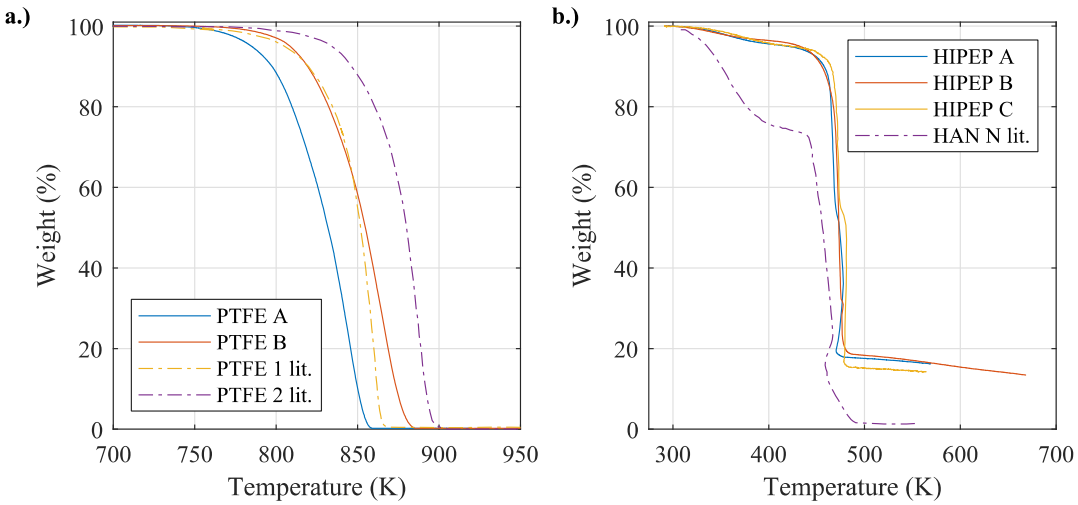

Figure 1: Thermogravimetric analysis curves for samples of a.) PTFE and b.) HIPEP.

Figure 1b shows the TGA curves for three samples of HIPEP. While there are no TGA data available for the HIPEP material in literature, data for aqueous HAN (called HAN N, 75% HAN, 25% H_2O) from Hoyani et al.[34] are also plotted here. The HAN N solution has a lower onset temperature than the HIPEP samples, but the main stage of thermal degradation for both materials occurs at a similar temperature of about 470 K. Both HIPEP and the HAN N solution of Hoyani et al.[34] exhibit a decrease in weight with increasing temperature for temperatures less than 470 K. This is due to the presence of and evaporation of water from the samples. HIPEP is known to be hygroscopic, absorbing 1-5% by mass of water from the atmosphere at typical laboratory humidity levels (~50%)[14], and the weight of HIPEP has decreased by about 5% when degradation begins at 470 K. The HAN N solution is 25% water and its weight has decreased by about 25% when degradation begins at 470 K. The final weight of HIPEP samples is greater than zero (~18%), indicating the samples do not completely degrade. A multiple-step degradation model is suggested by the TGA curve shape below 60%. This is marked by an endothermic reaction causing a decrease in temperature during the final stages of thermal degradation of HIPEP, between 450 and 500 K. This endothermic reaction is also observed in the same temperature range in the HAN data of Hoyani et al.[34]. The degradation curve of PTFE is smooth indicating a single-step degradation, whereas the degradation curve of HIPEP is unsteady, indicating multiple steps in the degradation process. The derivative of sample weight with respect to temperature was also examined to determine thermal degradation temperature. Specifically, we report the temperature of the inflection point at the maximum change in sample weight per unit change in temperature (i.e. the temperature at which sample mass is changing fastest). This temperature will be referred to as the degradation temperature. Table II presents the degradation temperature for each of the five samples tested using TGA along with results from literature.

Table II: Degradation temperatures for material samples during thermogravimetric analysis.

Sample	Initial mass, mg	Heating rate, K/min	Onset Temperature, K	Degradation Temperature, K
PTFE A	22.78	10	758	844
PTFE 1 lit.[33]	25.00	10	763	858
PTFE B	21.76	20	777	864
PTFE 2 lit.[33]	25.00	20	783	888
HIPEP A	21.54	10	430	468
HIPEP B	9.79	10	419	473
HIPEP C	20.15	20	438	473
HAN N lit.[34]	10.00	10	445	471

Despite the observation of a multi-step degradation of HIPEP, the variation in degradation temperature is less than 5 K for the three samples tested. The degradation temperature of HIPEP is about 473 K, compared to the 850 K degradation temperature of PTFE. Onset and thermal degradation temperatures increase with heating rate for PTFE as seen in our results as well as in literature. This is not true for HIPEP. The results of the PTFE testing are consistent with existing literature, and deviations of less than 3% in temperature can be attributed to the use of air as background

gas in the literature results, instead of the inert nitrogen environment used in the present work. Our measurement of degradation temperature for HIPEP is only 2 K different from an aqueous HAN sample tested in literature. However, HIPEP samples do exhibit an onset temperature of up to 26 K lower than the HAN. Based on these measurements, the low temperature bounds for PTFE and HIPEP were chosen as 900 K and 500 K, respectively.

B. Chemical Composition of PTFE Vapor

Using the described thermochemical modeling approach, the mole fractions of 19 gaseous chemical species were determined as a function of the equilibrium vapor temperature. One mole of propellant vapor was assumed in this analysis to be comprised entirely of the C_2F_4 molecule as shown in Table I, and the mole fractions were then converted to number densities and are displayed in Figure 2 for the temperature range of 900-40,000 K.

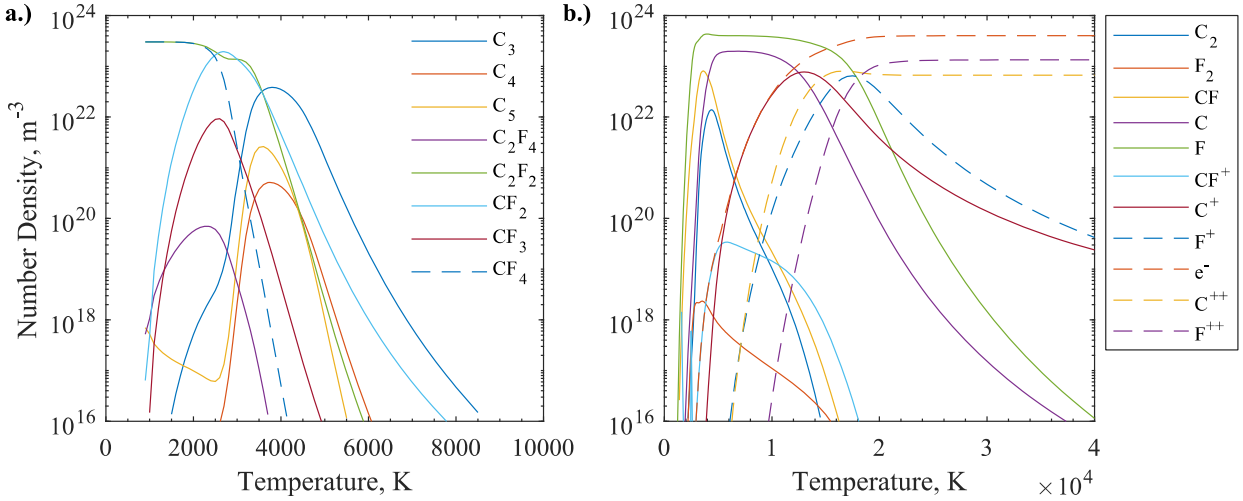

Figure 2: Equilibrium composition of 1 mol PTFE vapor at 1 bar pressure as a function of equilibrium temperature organized by a.) polyatomic and b.) atomic/ionic species.

From Figure 2, at low temperatures less than 2,000 K, the vapor is dominated by CF_4 and C_2F_2 species. Dissociation of the monomers into C_x, CF_x, F_2, and then subsequently into atomic C and F species, is rapid in the 2,000-4,000 K regime. Above 4,000 K these atomic neutrals are dominate and the vapor is nearly fully dissociated. The ionization energy of the Carbon atom is 11.26 eV compared to 17.42 eV for Fluorine. Thus, the onset of C^+ occurs around 8,000 K and peaks at 13,000 K compared to the higher onset at 10,000 K and peak at 17,500 K for F^+. With the increase in ionized species, the electron density predictably increases to a value of ~4×10^{23} m^{-3} at around 21,000 K and increases only marginally with increased temperature. At high temperatures above 21,000 K (~2 eV) the vapor is a strongly ionized plasma dominated by charged species C-II, F-II, C-III, F-III and electrons. Further increase in temperature to 40,000 K results in increased densities of the doubly ionized species and electrons corresponding to decreased singly ionized species densities.

To verify the regimes observed in the results from our model, we have compared to those presented in literature. The low temperature regime (<2,000 K) was shown to be dominated by CF_4 and C_5 by two other models[21,22]. In our model, C_5 is replaced by C_2F_2 but the vapor is also dominated by CF_4. Both models then show that dissociation leads to rapid increases in CF_2, CF, and atomic F above 2,200 K. Zhang et al.[22] shows F as the dominant species between ~3,500 K to the 7,000 K maximum temperature examined, with CF and C prevalent within this regime. The present work shows a dissociation regime very similar to this for PTFE vapor. H. Wang et al.[21] states that atomic fluorine is the most dominant species between 3,200 and 16,000 K, which is also observed in Figure 2. Further agreement with H. Wang et al. is observed for temperatures of 20,000 to 40,000 K where electrons are the most abundant species, followed by singly- and doubly-ionized carbon and fluorine. Kovitya[20] also reported predictions of ionization of C and F occurring at ~15,000 K with electrons and these ions dominating the vapor up to 30,000 K. In summary, the model presented here agrees well with the reported literature on the thermochemical composition of PTFE vapor.

C. Low Temperature HIPEP Combustion

Previously, a thermochemical model was developed and used to predict the equilibrium combustion temperature and product species of a variant of the HIPEP material [3]. As this is the only other known application of such a model to this material, it is prudent to compare with those results. The predicted mass fractions of the five most prevalent species are compared between the previous model [3] and the model presented here. The previous model results are

only available for 700 K and are presented in Table III. Qualitative agreement within 10% is observed, the five most abundant species are identical, and the relative order of abundance is nearly identical. The model presented here matches within 1% for N_2, CO, and H_2, though the order of abundance for CO and H_2 is reversed. While both models predict H_2O and CO_2 as the most and second-most abundant species, our model predicts ~7% more CO_2 by mass, and is the largest discrepancy between the two results. Our model also predicts 5.8% less H_2O than the previous model. It is noted that our lower predicted mass fraction of H_2O may be attributed to the hygroscopic nature of the propellant, which we have ignored in the present work. Samples of HIPEP are known to absorb 1-5% mass of water from the atmosphere if the relative humidity is at typical laboratory levels (~50%)[14]. It is unknown if Sawka and McPherson included this absorbed moisture in their analysis.

Table III: Comparison of predicted HIPEP composition at 700 K for two thermochemical models.

Species	Sawka & McPherson[3] Mass Fraction	This Work Mass Fraction
H_2O	43.62%	37.84%
CO_2	29.30%	36.32%
N_2	24.22%	23.62%
CO	1.07%	0.42%
H_2	0.11%	0.72%

V. Results and Discussion

Results from the model are presented with discussion of the significance. First, the chemical composition of the electric solid propellant vapor is detailed. Discussion of the predicted transport properties follows. Finally, a brief discussion of the observed trends in the model predictions is presented.

A. Chemical Composition of HIPEP Vapor

Using the propellant makeup model detailed in Table I, the thermochemical model was applied to determine the equilibrium mole fractions of 22 gas species comprising HIPEP vapor for a range of temperatures. The results of this prediction were converted to number density for one mole of vapor, and are shown in Figure 3 for the temperature range of 500-40,000 K.

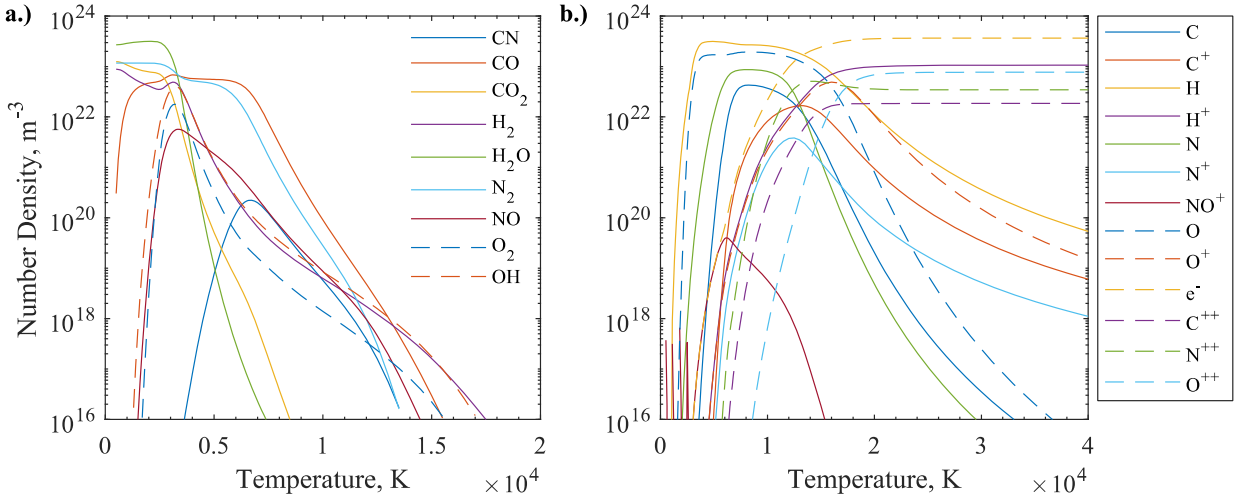

Figure 3: Equilibrium composition of 1 mol HIPEP vapor at 1 bar pressure as a function of equilibrium temperature organized by a.) polyatomic and b.) atomic/ionic species.

The general trends observed for PTFE hold for the predicted species in HIPEP vapor. At low temperatures below 3,000 K the vapor is dominated by the polyatomic species of H_2O, N_2, CO_2, and H_2. Above 3,500 K the dissociation of CO_2 incites an increase in the fraction of CO molecules, and H_2 is dissociated into atomic hydrogen. In the 5,000 to 10,000 K regime the vapor is largely comprised CO, N_2, N, H, and O. Further dissociation of CO and N_2 occurs in the 10,000 to 15,000 K regime in addition to ionization of H^+ and the coinciding increase in electron density. Above 18,000 K the HIPEP vapor is entirely dissociated and made up entirely of monatomic and ionic species. Ionization

(and electron density) increases with further increase in temperature. At high temperatures of 25,000 K or more, the HIPEP vapor is strongly ionized and comprised of mainly single protons and electrons in addition to large populations of O-III, N-III, and C-III.

B. Transport Properties

Using the approach detailed by Gordon et al.[29] and included in the NASA CEA program, the viscosity and thermal conductivity of both HIPEP and PTFE vapor were determined. The calculation of the mixture viscosity is entirely dependent on the individual neutral species viscosity. Neutral gas viscosity is proportional to $T^{1/2}$ and inversely proportional to the collision integrals, which decrease with temperature. Thus, a constant proportionality to temperature is generally observed in Figure 4 up to 12,000 K. A deviation from this dependence occurs in the 12,000 to 18,000 K regime for both material vapors. In this region, ionization begins. While ion densities remain low relative to monatomic neutrals, electron density increases to the order of monatomic species. The viscosity contribution of electrons is very low relative to monatomic neutrals, and thus a negative dependence on T is observed in this regime. For PTFE, electrons become the most abundant species at ~15,000 K whereas for HIPEP electrons become dominant at ~12,500 K, which is the reason for the higher onset temperature for this negative dependence in PTFE vapor. Other thermochemical models show a continued decrease in mixture viscosity for PTFE vapor with further increase in temperature[20-22]. The present work differs in that we do not consider the Coulomb interaction, which is stronger than the neutral-neutral interaction that is considered in viscosity calculation. This Coulomb interaction decreases viscosity and becomes prevalent when ion densities are high, in this case, temperatures above 20,000 K for both material vapors. As a result, predictions for viscosity in the high temperature regime do not agree with literature results for PTFE. Future efforts will need to include the Coulomb interaction for accurate viscosity prediction in this strongly ionized regime. Mixture viscosity is not critical to ablation models, so the likely inaccuracies in the high temperature regime are not a major concern for current and near-term ablation model work.

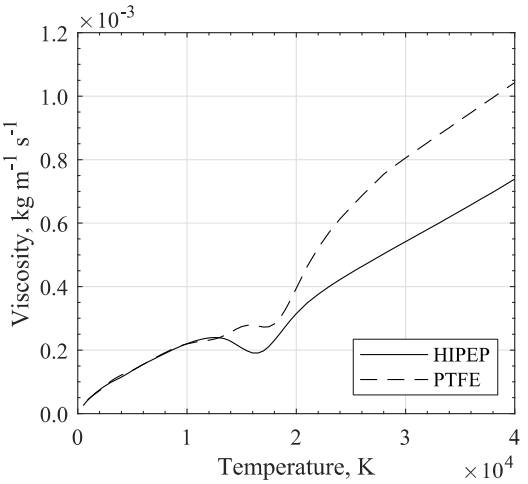

Figure 4: Predicted viscosity of HIPEP and PTFE vapors as a function of equilibrium temperature.

Total thermal conductivity of HIPEP and PTFE vapors are shown in Figure 5. At low temperatures less than 3,000 K where the gas is dominated by heavy neutral species, the conductivity greatly increases with temperature for both vapors to the on the order of 1 W/m/K because of increased translation of these species. Above 3,000 K up to 20,000 K dissociation and ionization take place on a large scale for both vapors and as a result the reaction contribution to thermal conductivity dominates the total conductivity. Thermal conductivity fluctuates from 1-10 W/m/K for both vapors in this regime with multiple peaks. Increase in the number density of doubly-ionized species greatly increases the reaction and heavy particle translation contributions to thermal conductivity. In this high temperature regime (>25,000 K) minimal fluctuations and nearly linear increase with temperature are observed in our prediction of the thermal conductivity for each material vapor. Comparison with Kovitya[20] shows agreement within 50% in the 5,000-10,000 K regime for thermal conductivity of PTFE vapor, but our prediction is a factor of about 5 greater between 11,000 and 20,000 K. Figure 5 also matches closely with that of Zhang et al.[22] for temperatures less than 10,000 K. The discrepancies in this high temperature regime are likely due to the present model neglecting the Coulomb interaction that would strongly affect the calculation of collision integrals when the degree of ionization is high.

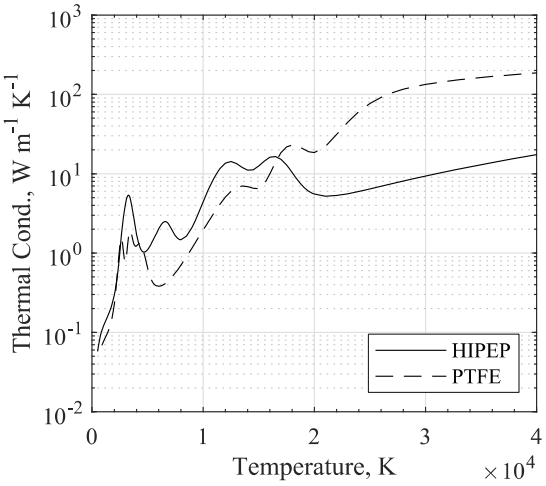

Figure 5: Predicted thermal conductivity of HIPEP and PTFE vapors with temperature.

Previous experimental work with the HIPEP material has focused on its differences from PTFE when used as propellant in pulsed plasma thrusters. Figure 4 and Figure 5 show similar trends in transport properties between the materials, but clear differences in magnitude are observed. Viscosity of the materials are within ~5% for temperatures less than 13,000 K, but differ by up to 8.8×10^{-5} kg/m/s (~40%) in the regime where electron density increases (12,000-20,000 K). In the high temperature regime, a separation of up to a factor of 1.4 in the viscosity of the vapors is observed, with PTFE vapor viscosity always greater than that of HIPEP. Conversely, HIPEP vapor thermal conductivity is always at least 10% greater than that of PTFE for temperatures <17,000 K, but PTFE vapor becomes more conductive at higher temperatures, by a factor of ~10.

VI. Conclusions

A thermochemical model was developed describing the composition and thermodynamic transport properties of an electric solid propellant vapor under equilibrium conditions. This model used the minimization of Gibbs free energy method to yield mole fractions of 22 individual gaseous species as a function of the equilibrium temperature. An approximate Chapman-Enskog method was employed to calculate the viscosity and thermal conductivity of the predicted gas mixture. This approach was also employed for PTFE vapor, and results were compared to those available in published literature. Results agree with multiple literature sources in terms of the dominant equilibrium species with respect to temperature. Transport property results also were found to agree to within an order of magnitude for temperatures up to 15,000 K.

In the low temperature regime, the vapor of the electric solid propellant HIPEP is dominated by polyatomic species H_2O, N_2, CO_2, CO, and H_2. The mass fractions of these species predicted by the model match within 10% to another researcher's predictions for an earlier formulation of the material at 700 K. Dissociation dominates between 3,500 K and 10,000 K, above which protons and electrons are formed from ionization of atomic hydrogen. Above 18,000 K HIPEP vapor is fully dissociated and weakly ionized. Strong ionization occurs above 25,000 K, with C, N, and O ions in the second ionization state mixed with free protons and electrons.

Transport property calculations indicate that HIPEP vapor has viscosity similar to PTFE vapor at low temperature (<15,000 K), but is less viscous at higher temperatures where dissociation is prominent. The viscosity of both vapors is on the order of 10^{-4} kg/m/s at temperatures below 15,000 K. Low temperature HIPEP vapor is predicted to be more thermally conductive than that of PTFE by 10-100%. When dissociation and ionization take over at the higher temperatures (>20,000 K), however, PTFE vapor thermal conductivity is predicted to be up to a factor of 10 larger than HIPEP.

Acknowledgments

M.S. Glascock is extremely grateful for the NASA Space Technology Research Fellows program, which funded this research under grant number NNX15AP31H. The authors thank Dr. John Yim at NASA Glenn Research Center for assistance with the CEA program and fruitful discussion on the work. The authors also thank Dr. Kurt Polzin of NASA Marshall Space Flight Center for his advice and discussion. The authors thank Digital Solid State Propulsion, LLC for HIPEP samples for TGA, as well as previous thermochemical modeling work on the material. Finally, the authors wish to thank Lou Ann Miller and Tim Spila at the University of Illinois for their assistance with the TGA.

References

[1]Sawka, W. N., "Pulse Performance and Power Requirements for Electrically Controlled Solid Propellant," *54th JANNAF Propulsion Meeting*, JANNAF, Denver, CO, 2007.

[2]Sawka, W. N., Katzakian, A., and Grix, C., "Solid State Digital Cluster Thrusters for Small Satellites, Using High Performance Electrically Controlled Extinguishable Solid Propellants," *AIAA/USU Conference on Small Satellites*, AIAA, Logan, UT, 2005.

[3]Sawka, W. N., and McPherson, M., "Electrical Solid Propellants: A Safe, Micro to Macro Propulsion Technology," *49th AIAA/ASME/SAE/ASEE Joint Propulsion Conference*, AIAA, San Jose, CA, 2013. doi: 10.2514/6.2013-4168

[4]Burton, R. L., and Turchi, P. J., "Pulsed Plasma Thruster," *Journal of Propulsion and Power,* Vol. 14, No. 5, 1998, pp. 716-735. doi: 10.2514/2.5334

[5]Antonsen, E. L., Burton, R. L., Reed, G. A., and Spanjers, G. G., "Effects of Postpulse Surface Temperature on Micropulsed Plasma Thruster Operation," *Journal of Propulsion and Power,* Vol. 21, No. 5, 2005, pp. 877-883. doi: 10.2514/1.13032

[6]Gatsonis, N. A., Juric, D., Stechmann, D., and Byrne, L., "Numerical Analysis of Teflon Ablation in Pulsed Plasma Thrusters," *43rd AIAA/ASME/SAE/ASEE Joint Propulsion Conference & Exhibit*, AIAA, Cincinnati, OH, 2007. doi: 10.2514/6.2007-5227

[7]Keidar, M., Boyd, I. D., Antonsen, E. L., Gulczinski III, F. S., and Spanjers, G. G., "Propellant Charring in Pulsed Plasma Thrusters," *Journal of Propulsion and Power,* Vol. 20, No. 6, 2004, pp. 978-984. doi: 10.2514/1.2471

[8]Mikellides, P., and Turchi, P., "Modeling of late-time ablation in Teflon pulsed plasma thrusters," *32nd Joint Propulsion Conference and Exhibit*, AIAA, Lake Buena Vista, FL, 1996. doi: 10.2514/6.1996-2733

[9]Ruchti, C. B., and Niemeyer, L., "Ablation Controlled Arcs," *IEEE Transactions on Plasma Science,* Vol. PS-14, No. 4, 1986, pp. 423-434.

[10]Schönherr, T., Komurasaki, K., and Herdrich, G., "Propellant Utilization Efficiency in a Pulsed Plasma Thruster," *Journal of Propulsion and Power,* Vol. 29, No. 6, 2013, pp. 1478-1487. doi: 10.2514/1.B34789

[11]Seeger, M., Tepper, J., Christen, T., and Abrahamson, J., "Experimental Study on PTFE Ablation in High Voltage Circuit-Breakers," *Journal of Physics D: Applied Physics,* Vol. 39, No. 23, 2006, pp. 5016-5024. doi: 10.1088/0022-3727/39/23/018

[12]Spanjers, G. G., Lotspeich, J. S., McFall, K. A., and Spores, R. A., "Propellant Losses Because of Particulate Emission in a Pulsed Plasma Thruster," *Journal of Propulsion and Power,* Vol. 14, No. 4, 1998, pp. 554-559. doi: 10.2514/2.5313

[13]Glascock, M. S., and Rovey, J. L., "Ablation Mass Loss of an Electric Solid Propellant in a Pulsed Plasma Thruster," *35th International Electric Propulsion Conference*, ERPS, Atlanta, GA, 2017.

[14]Glascock, M. S., and Rovey, J. L., "Electric Solid Propellant Ablation in a Pulsed Electric Thruster," *2018 Joint Propulsion Conference, AIAA Propulsion and Energy Forum*, AIAA, Cincinnati, OH, 2018.

[15]Glascock, M. S., Rovey, J. L., Williams, S., and Thrasher, J., "Plasma Plume Characterization of Electric Solid Propellant Micro Pulsed Plasma Thrusters," *51st AIAA/SAE/ASEE Joint Propulsion Conference*, AIAA, Orlando, FL, 2015. doi: 10.2514/6.2015-4185

[16]Glascock, M. S., Rovey, J. L., Williams, S., and Thrasher, J., "Observation of Late-Time Ablation in Electric Solid Propellant Pulsed Microthrusters," *52nd AIAA/SAE/ASEE Joint Propulsion Conference*, AIAA, Salt Lake City, UT, 2016. doi: https://doi.org/10.2514/6.2016-4845

[17]Glascock, M. S., Rovey, J. L., Williams, S., and Thrasher, J., "Characterization of Electric Solid Propellant Pulsed Microthrusters," *Journal of Propulsion and Power,* Vol. 33, No. 4, 2017, pp. 870-880. doi: 10.2514/1.B36271

[18]Keidar, M., Boyd, I. D., and Beilis, I. I., "Electrical Discharge in the Teflon Cavity of a Coaxial Pulsed Plasma Thruster," *IEEE Transactions on Plasma Science,* Vol. 28, No. 2, 2000, pp. 376-385.

[19]Keidar, M., Boyd, I. D., and Beilis, I. I., "Model of an Electrothermal Pulsed Plasma Thruster," *Journal of Propulsion and Power,* Vol. 19, No. 3, 2003, pp. 424-430. doi: 10.2514/2.6125

[20]Kovitya, P., "Thermodynamic and Transport Properties of Ablated Vapors of PTFE, Alumina, Perspex, and PVC," *IEEE Transactions on Plasma Science,* Vol. 12, No. 1, 1984, pp. 38-42.

[21]Wang, H., Wang, W., Yan, J. D., Qi, H., Geng, J., and Wu, Y., "Thermodynamic Properties and Transport Coefficients of a Two-Temperature PTFE Vapor Plasma," *Journal of Physics D: Applied Physics,* Vol. 50, No. 39, 2017.

[22]Zhang, J. L., Yan, J. D., Murphy, A. B., Hall, W., and Fang, M. T. C., "Computational Investigation of Arc Behavior in an Auto-Expansion Circuit Breaker Contaminated by Ablated Nozzle Vapor," *IEEE Transactions on Plasma Science,* Vol. 30, No. 2, 2002, pp. 706-719.

[23]Gordon, S., and McBride, B. J., "Computer Program for Calculation of Complex Chemical Equilibrium Compositions and Applications," *NASA Reference Publication,* Vol. 1311, 1994.

[24]McBride, B. J., and Gordon, S., "Chemical Equilibrium with Applications," 02/04/2016, https://www.grc.nasa.gov/www/CEAWeb/
[25]Chase, M. W., "NIST-JANAF Thermochemical Tables, Fourth Edition," *Physical and Chemical Reference Data*, 1998.
[26]Vincenti, W. G., and Kruger, C. H., *Introduction to Physical Gas Dynamics*: Krieger Publishing Co., 1965.
[27]Kramida, A., Ralchenko, Y., and Reader, J., *NIST Atomic Spectra Database (ver. 5.5.6)*, 2018.
[28]Hirschfelder, J. O., Curtiss, C. F., and Bird, B. B., *Molecular Theory of Gases and Liquids*, 1954.
[29]Gordon, S., McBride, B. J., and Zeleznik, F. J., "Computer Program for Calculation of Complex Chemical Equilibrium Compositions and Applications, Supplement I-Transport Properties," *NASA TM-86885*, 1984.
[30]Svehla, R. A., and McBride, B. J., "Fortran IV Computer Program for Calculation of Thermodynamic and Transport Properties of Complex Chemical Systems," *NASA TN D-7056*, 1973.
[31]Schild, H. G., "Application of TGA/ FTlR to the Thermal Degradation Mechanism of Tetrafluoroethylene-Propylene Copolymers," *Journal of Polymer Science A: Poly. Chem.,* Vol. 31, 1993, pp. 1629-1632.
[32]Lee, H., and Litzinger, T. A., "Chemical Kinetic Study of HAN Decompostion," *Combustion and Flame,* Vol. 135, No. 2, 2003, pp. 151-169.
[33]Hondred, P. R., Yoon, S., Bowler, N., and Kessler, M. R., "Degradation Kinetics of Polytetrafluoroethylene and poly(ethylene-alt-tetrafluoroethylene)," *High Performance Polymers,* Vol. 25, No. 5, 2013, pp. 535-542. doi: 10.1177/0954008312473491
[34]Hoyani, S., Patel, R., Oommen, C., and Rajeev, R., "Thermal Stability of Hydroxylammonium Nitrate (HAN)," *Journal of Thermal Analysis and Calorimetry,* Vol. 129, 2017, pp. 1083-1093.